Patterning Nanostructured, Synthetic, Polymeric Receptors by Simultaneous Projection Photolithography, Nanomolding, and Molecular Imprinting

Ana V. Linares, Aude Falcimaigne-Cordin, Levi A. Gheber, and Karsten Haupt**

***M**icroscope projection photolithography is combined with nanomolding and molecular imprinting for the fast microfabrication of molecularly imprinted polymer (MIP) arrays in the form of micrometric islands of nanofilaments. Dot diameters from 70–90 μm are easily obtained using a 10× objective and a photomask carrying the desired pattern. The dots are composed of parallel nanofilaments of a high aspect ratio, 150 nm in diameter and several micrometers in length, which are obtained through a nanomolding procedure on porous alumina. The arrays are molecularly imprinted with the small molecule fluorescein or with the protein myoglobin. The fluorescein MIP arrays are able to specifically recognize their target, as demonstrated by fluorescence microscopy. A four-fold increase in binding capacity and imprinting factor (IF = 13) is obtained compared to non-nanostructured porous dots. Imprinting of the nanofilament arrays with the protein myoglobin as the template is also possible and allows for a high imprinting factor of 4.3. Such nanostructured microarrays of synthetic receptors obtained by projection photolithography have great potential in biosensor and biochip development.*

1. Introduction

Biochips are arrays of biomolecules locally immobilized on a surface like glass or silicon.[1,2] Their applications include molecular screening, environmental analysis, and clinical testing.[3,4] The recognition elements in biochips and biosensors are most commonly biomacromolecules such as enzymes, antibodies, or DNA. However, these are often unstable when used out of their natural environment, they may require conservation at low temperatures, and may not be compatible with certain standard industrial fabrication procedures. Therefore, synthetic biomimetic receptors like molecularly imprinted polymers (MIPs) are being evaluated as an alternative.[5,6] MIPs are produced by a templating process at the molecular level. They are able to bind target molecules with similar affinity and specificity to those of their natural counterparts. Their superior stability facilitates their use even in severe environments.

For the development of biochips based on MIPs, the latter have to be patterned on a substrate. For quite some time, photolithographic methods have been extensively employed for microfabrication in the semiconductor industry, however, since the early 90's these techniques have also played an important role in biosensor technology as a method of interfacing a recognition element (oligonucleotides, peptides, proteins, and cells) with the surface of a transducer resulting in well-defined micropatterned arrays. Advanced microfabrication techniques have been developed such as scanning-beam and projection lithography.[7] Microscope projection photolithography (MPP) was first developed in 1973 by Palmer and Decker, who used a reflection microscope equipped with a vertical illuminator to project the desired pattern on a photoresist layer for the fabrication of refractory superconducting

Dr. A. V. Linares, Dr. A. Falcimaigne-Cordin, Prof. K. Haupt
Compiègne University of Technology
UMR CNRS 6022, BP 20529, 60205 Compiègne, France
E-mail: karsten.haupt@utc.fr
Dr. L. A. Gheber
Department of Biotechnology Engineering
Ben-Gurion University of the Negev
Beer-Sheva 84105, Israel
E-mail: glevi@bgu.ac.il

DOI: 10.1002/smll.201100248

NANO MICRO small

films.[8] This proved to be a facile method, where the mask is placed in the same plane as the field diaphragm of the microscope and the image is demagnified by the nominal power of the objective.

For large-scale production, photolithography requires high-precision photomasks including mask writers and aligners, contamination-free environments, and other expensive equipment. However, the possibility of quickly obtaining prototypes through MPP, where the photomask can be fabricated by simply printing the motif of interest onto an overhead transparency, appears attractive as it offers a fast and inexpensive means of optimization in the stages of exploratory research. Indeed, MPP has been successfully utilized to pattern a variety of materials such as self-assembled alkanethiol monolayers,[9] fluorescently-labeled supported lipid bilayers[10] and also commercial photoresists (Microposit 1805 and 1813, SU-8) for the preparation of masters for soft lithography.[11]

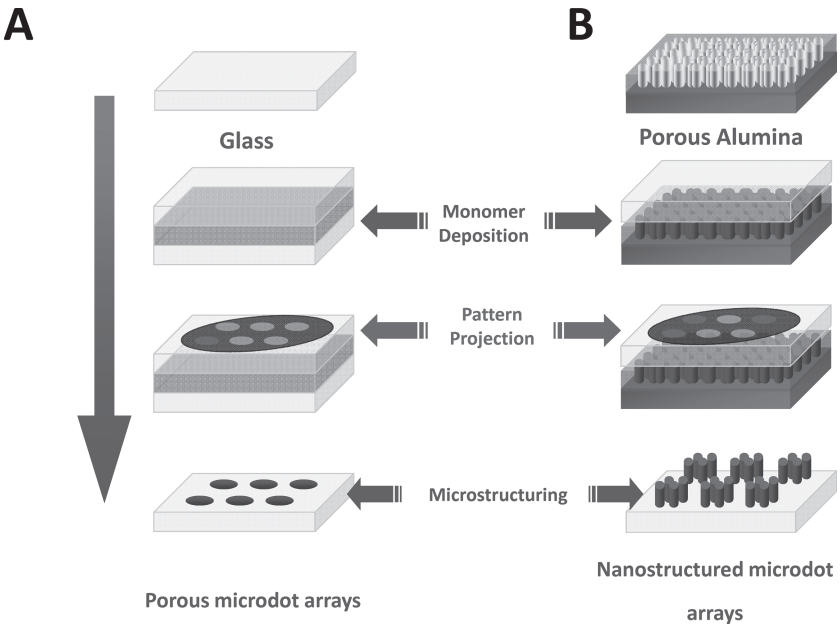

Figure 1. Schematic representation of MPP for the preparation of A) porous microdot arrays and B) nanofilament microdot arrays.

The use of photolithographic methods has also been reported in conjunction with various molecular imprinting strategies, where MIP precursor solutions have been used as photoresists. Laser-beam (maskless) photolithography was, for example, employed by Shea and co-workers who obtained 3D MIP microstructures using a UV-laser beam and Tinuvin as an additional UV absorber in the MIP precursors mixture.[12] A noteworthy example of microfabrication combined with MIPs for chip technology was reported by Huang et al. where UV-mask lithography was utilized for MIP patterning onto Pt electrodes. This ultimately allowed the assembly of an electrochemical sensor array for the detection of the anabolic steroid albuterol.[13,14] However, the standard MIP recipe was modified in this case with the use of polynorborene, acrylic copolymers as functional monomers, and carbon paste as an additive to increase the electrical conductivity. Wafer-scale mass production of MIP microchips at micrometer resolution has been reported recently by Ayela and co-workers.[15]

Since the binding sites in an MIP are normally buried in the polymer matrix, access may sometimes be difficult, particularly for large molecules like proteins. In order to improve the accessibility of the imprinted binding sites in MIP microdots, it has been suggested that their porosity may be improved by the addition of a sacrificial polymeric porogen.[16,17] This has been shown effective for small target molecules. For protein targets, we anticipate that nanostructured surfaces with a high aspect ratio will have advantages over porous films, since pore diffusion is avoided and mass transfer improved.[18] In the present work, we describe the synthesis of MIP microdot arrays on glass slides by projection photolithography, both in the form of porous dots and as islands of polymer nanofilaments by nanomolding on anodized alumina (**Figure 1**). The latter approach has the additional advantage that the template molecule can be immobilized on the nanoporous alumina prior to MIP synthesis, thus creating imprinted sites only in the surface of the filaments. This will greatly improve the mass transfer and binding kinetics when these MIPs are used in biochips and sensors.

2. Results and Discussion

2.1. MIP Synthesis by Microscope Projection Photolithography

The performance of MPP for the fabrication of molecularly imprinted polymer arrays was evaluated in terms of the linear factor of reduction and the obtained resolution. In order to produce the pattern, the photomask inserted in the field-diaphragm plane of the microscope is projected onto the MIP precursors mixture. Generally, the achieved size reduction is proportional to the magnification of the objective used, although this will also depend on additional microscope optics. **Figure 2** shows an example of a photomask where a relatively large distance between dots was chosen (Figure 2A), and the resulting polymer pattern on a glass support, after projection of the mask with a 10× objective onto the MIP precursor solution (Figure 2B). The dimensions of the squares in the photomask are 0.5 mm; they are reduced by a linear factor of 7 in the resultant polymeric array. The linear factor of reduction is smaller than the nominal magnification of the objective (10×), which is due to a combination of factors related to the optics of the microscope[11] and the uncontrolled diffusion of radicals during irradiation that leads to polymerization even after the light source is turned off.

The resolution limit (R) is set by the theoretical limits of diffraction (Rayleigh criterion) and is described by

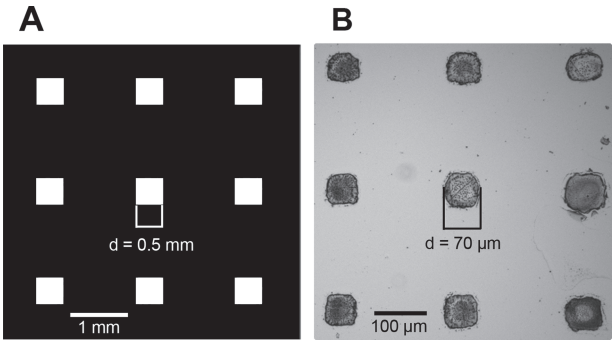

Figure 2. Correlation between the designed pattern of the photomask and the obtained polymeric array. A) scaled picture of the transparent photomask; B) bright-field microscopy image of the polymer dot array. Patterns were obtained using a mask with 0.5 mm × 0.5 mm features and a pitch of 2 mm.

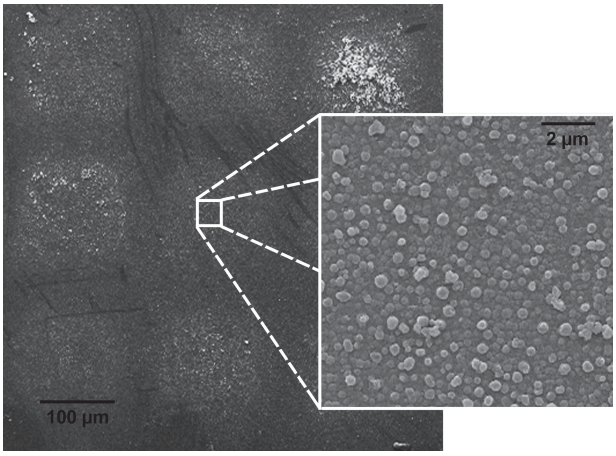

Figure 3. SEM image of a dot array section obtained at 150× magnification. The inset with 5000× magnification reveals the surface morphology of the dot.

Equation (1) where NA is the numerical aperture of the microscope objective (0.2), and λ the wavelength of the light source:

$$R = 0.61\lambda/NA \quad (1)$$

In our case, the light source is the Hg lamp from the microscope with an IR mirror, which means that the emission wavelength range is 230–700 nm. To calculate the highest resolution limit of our setup, 700 nm was considered as the λ value. Thus, the resolution limit of our setup is R = 2.1 µm, considerably lower than the size of the dots (70 µm). For practical reasons of detection, and in order to maintain a large view field, we used masks with patterns of 0.5 mm × 0.5 mm features and pitches of 1 or 2 mm, and a 10× objective, resulting in 70–90 µm dots. The dot arrays were characterized by scanning electron microscopy (SEM) (**Figure 3**). Their surface reveals aggregated nanoparticles, a morphology relatively common with polymers synthesized by free-radical polymerization in a bad solvent. The size of the domains varies from 100–500 nm approximately.

In the case of nanofilament dot arrays (**Figure 4**), single nanofilaments can be clearly observed at higher magnification. The diameter of the dot is approximately 90 µm. The nanofilament dots are slightly larger than the microporous dots when the same mask is used, due to the fact that the surface of the aluminium underneath the porous oxide on which the projected pattern is not ideally flat. Therefore, some diffuse reflection occurs that results in slightly larger dots than in the case of the microporous dots where projection is onto a flat and transparent glass surface. The dots are composed of nanofilaments with a diameter of 150 nm. The length of the nanofilaments determines the thickness of the dot. In Figure 4B one can observe the full length of a few nanofilaments that have detached from the dot, approximately 4 µm. These dimensions correspond well to the dimensions of the mold, which indicates virtually full polymerization of the monomer mixture in the alumina pores. Thus, MPP yields similar results as those obtained by nanomolding the entire area of the substrate without patterning.[19] In fact, for the present work we have used alumina oxides yielding the above dimensions of filaments (see Experimental Section), but filaments with different dimensions are easily accessible with this technique, having diameters between 30 and 250 nm, and lengths between 500 nm and 10 µm.[19] Concerning the stability of the nanofilament dot arrays over time, we have not observed any degradation of the arrays even after repeated incubation and regeneration cycles over several months.

2.2. Recognition Properties of MIP Arrays

The recognition properties of the fluorescein-imprinted porous microdot arrays were tested by direct measurement of the fluorescence intensity of the arrays after template adsorption. These intensity values were calculated from the fluorescence microscopy images. The fluorescence intensities of the MIP and the nonimprinted control polymer (NIP) arrays were measured at three different

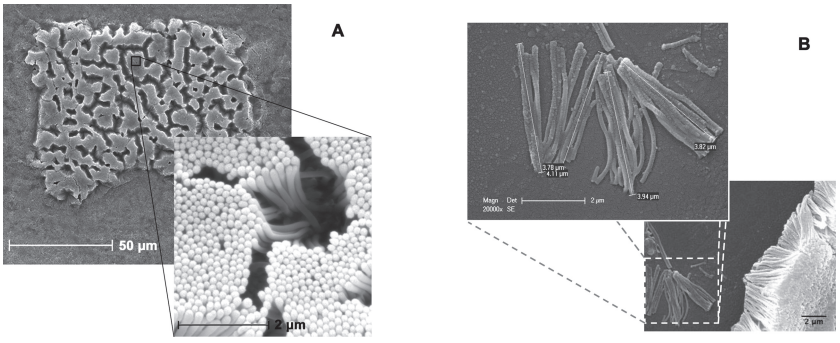

Figure 4. A) SEM image of a single nanofilament dot (magnification: 750×, inset: 20000×); B) SEM image of the edge of a nanofilament dot (magnification 5000×, inset: 20000×).

small NANO MICRO

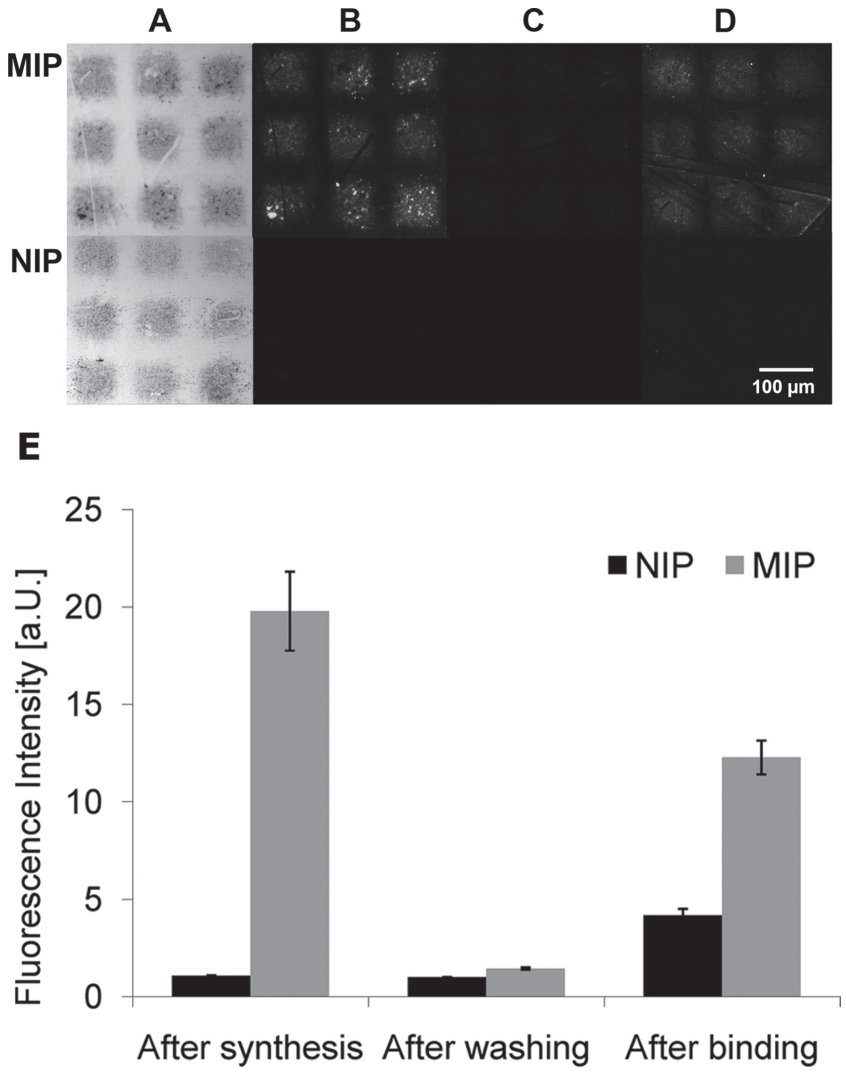

Figure 5. Optical images of fluorescein-imprinted and nonimprinted arrays of porous dots. Patterns were obtained using a mask with 0.5 mm × 0.5 mm features and a pitch of 1 mm. A) bright-field images; B) fluorescence images following synthesis; C) fluorescence images after fluorescein removal; D) fluorescence image after fluorescein adsorption (75 μM in DMSO). Exposure time: 350 ms. E) Quantitative representation of the fluorescence intensities extracted from the images in B, C, and D. Measurements were done in triplicate, and the error bars represent the standard error of the mean.

stages: after synthesis, after removal of the template, and after re-adsorption of fluorescein (**Figure 5**). The fluorescence images obtained after synthesis of MIP and NIP arrays and after template removal (Figure 5B,C) show that the fluorescence detected was due to the template, and that the template can be effectively removed from the MIP. Following incubation of the arrays with a solution of fluorescein (Figure 5D), emission intensity values from the MIP array are obtained similar to those after synthesis, while little fluorescence was detected on the NIP surface. The measured intensity values are shown in Figure 5E. As can be seen, 92% of the initial fluorescence was eliminated after the washing procedure and a recovery of 62% with respect to the initial value was achieved after incubation with 75 μM fluorescein. The imprinting factor (IF) is 3. Repeated incubation and wash cycles resulted in a very low variation of the measured intensity values (within 10%).

In order to verify the specificity of the imprinted binding sites, competitive binding assays with a nonfluorescent structural analogue of fluorescein, fluorescein diacetate (**Figure 6**), were performed. The samples were incubated with increasing concentrations of fluorescein diacetate, keeping the concentration of fluorescein constant at 20 μM (Figure 6C). The results show a low but significant decrease in fluorescence in the MIP, which is dependent on the concentration of the competitor. The weak competition is probably due to the additional acetate groups that prevent correct positioning of the molecule in the imprinted binding sites. Virtually no competition is observed in the NIP. This demonstrates at the same time the potential use of these arrays in biochips based on competitive assay formats with fluorescent labels.

Nanofilament dot arrays obtained by nanomolding on nanoporous alumina substrates, imprinted with fluorescein and myoglobin, were also tested for their binding properties. Before imprinting, the template was immobilized on the walls of the alumina pores to achieve a better homogeneity and accessibility of the binding sites formed during the polymerization process. In **Figure 7** one can observe the arrays of nanofilament dots obtained with fluorescein as the template. The pattern is not clearly observable in the bright-field images (Figure 7A), probably due to light scattering on the filaments, however, it is clearly revealed in the fluorescence images obtained with the same microscope (Figure 7B,C,D). Fluorescence images were taken after synthesis, after template removal, and after incubation with fluorescein (20 μM). Figure 7E shows that a significant decrease in fluorescence intensity was achieved following extraction of the template, however, some template remains trapped in the polymer. This may be due to some fluorescein being only physically adsorbed in the pores of the alumina, becoming entrapped in the nonporous polymer matrix of the nanofilaments. In all binding experiments, the fluorescence intensity values of the MIP arrays were therefore corrected for this background fluorescence. The higher fluorescence intensity after the binding experiments compared to the values after synthesis is due to the fact that during the dissolution of the aluminium/alumina substrate some of the fluorescein is inevitably washed out from the nanofilaments, thus the intensity value after synthesis corresponds to only part of the amount of template originally used.

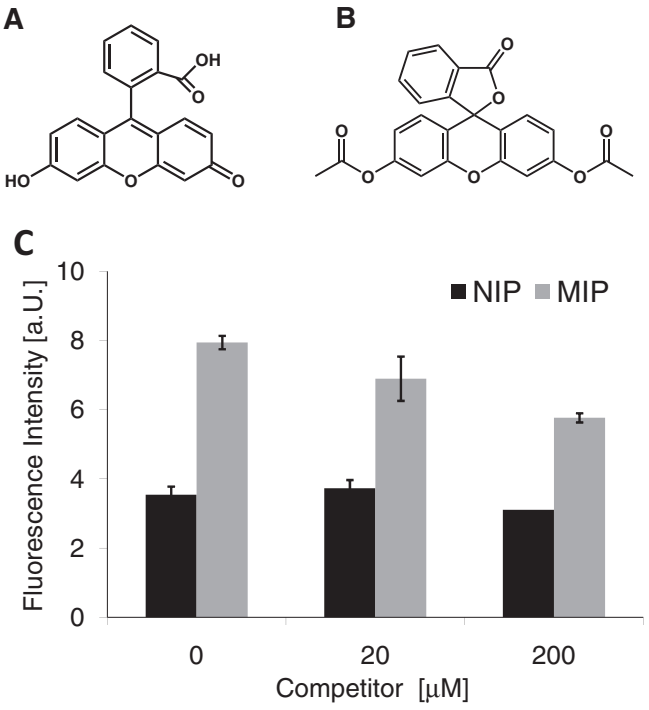

Figure 6. Chemical structures of A) the template molecule fluorescein and B) its nonfluorescent structural analogue, fluorescein diacetate. C) Fluorescence intensity values for the fluorescein-imprinted MIP and NIP arrays (porous dots) at a fixed concentration of template (20 μM), and at two different concentrations of the fluorescein diacetate competitor. Measurements were done in triplicate, the error bars represent the standard error of the mean.

The main advantage of the use of nanofilament dot arrays as compared to plain porous dots is the increase in the active surface area of the array combined with the greater accessibility of the binding sites, since they are located at or close to the surface of the nanostructures. Indeed, when comparing the binding experiments with plain porous dots and nanofilament dots, the fluorescence intensity values of the nanofilament MIP dots are about four times higher than those of the plain porous dots, and the imprinting factor also increases to 13 (as compared to 3 in the case of plain dots).

2.3. Protein Imprinting

The same approach was used as described above for the imprinting of myoglobin in nanofilament dot arrays. One of the major drawbacks in protein imprinting is the accessibility of the recognition cavities for the target protein, if the cavities are buried in the polymer matrix. In earlier publications, it has therefore been suggested to use immobilized template proteins for imprinting, in order to localize the recognition cavities at the polymer surface.[18] At the same time, this solves possible solubility problems of the protein in the MIP precursors mixture.

Myoglobin imprinted nanofilament arrays were prepared by MPP after immobilization of the protein in the nanoporous alumina substrates. Bright-field images of typical arrays are shown in **Figure 8**A. The diameter of the dots is approximately 80 μm. The dots were then incubated in solutions of FITC-labeled myoglobin at 1 μM concentration. The fluorescence images (Figure 8B,C) show an increase in fluorescence intensity after FITC–myoglobin binding. After extracting quantitative fluorescence intensity values from the images, an IF of 4.3 was obtained under these conditions. In order to test for selectivity of the MIP, the binding of two other proteins, hemoglobin and cytochrome C, was studied. While cytochrome C showed slightly higher nonspecific binding (by 20%) than myoglobin, no specific binding was obtained (IF = 0). In the case of hemoglobin, the nonspecific binding was slightly lower than that of myoglobin, and a minor imprinting effect was observed (IF = 1.5). These results indicate that the MIP is indeed specific for myoglobin.

3. Conclusion

Microscope projection photolithography combined with nanomolding and molecular imprinting has been successfully used for the fast microfabrication of MIP arrays in the form of porous dots and dots composed of nanofilaments. Arrays with dot diameters from 70–90 μm were easily obtained using a 10× objective and a photomask with the desired pattern printed on acetate film. Further reduction of the size of the array will be possible with higher magnification objectives, while the resolution may be improved with objectives with a higher NA. The dots were composed of parallel nanofilaments of 150 nm diameter and 4 μm length obtained through a nanomolding procedure on porous alumina. The recognition properties of the arrays imprinted with the small molecule fluorescein and with the protein myoglobin were tested by fluorescence microscopy in direct and competitive-binding assays. In the case of the fluorescein MIP, an increase in binding capacity and in imprinting factor (IF = 13) was obtained when using nanofilament dots instead of porous dots. Imprinting of the nanofilament dot arrays with the protein myoglobin as the template was also achieved with an imprinting factor of IF = 4.3. Such nanostructured microarrays of synthetic receptors obtained by projection photolithography will have a great potential for use in biosensors and biochips, due to their straightforward synthesis, economic production, chemical and physical stability, together with specific molecular-recognition properties.

4. Experimental Section

Reagents: aluminium sheet rolls (30 mm × 0.3 mm, 99.99% purity) were obtained from Merck and polished microscope glass slides of (76 mm × 26 mm × 1 mm) were purchased from Menzel-Glaser. (3-aminopropyl)triethoxysilane (APTES), methacryloylamidopropyl trimethoxysilane (MAPTMS) and glutaraldehyde, were from Sigma-Aldrich. Methyl methacrylate (MMA), methacrylic acid (MAA), hydroxyethylmethacrylate (HEMA), 4-vinyl pyridine (4-VPy), triethylenglycol dimethacrylate (TEDMA), trimethylol-propane trimethacrylate (TRIM), poly(vinyl acetate) (PVAc) (average molecular weight 140 000 g mol^{-1}) and 2,2-dimethoxy-2-phenyl-acetophenone (DPAP)

NANO MICRO small

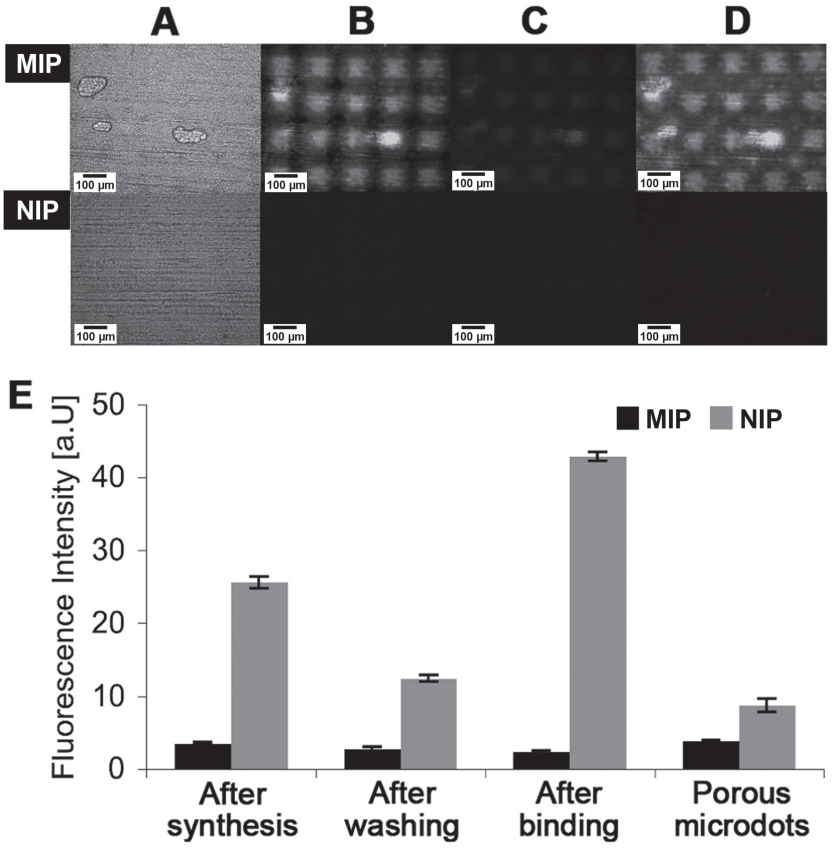

Figure 7. Optical images of fluorescein MIP and NIP arrays of nanofilament dots. Patterns were obtained using a mask with 0.5 mm×0.5 mm features and a pitch of 1 mm. A) bright-field images; B) fluorescence images directly after synthesis and mould removal; C) fluorescence images after removal of the template; D) fluorescence image after fluorescein (20 µM) adsorption in DMSO. Exposure time: 380 ms. E) Fluorescence intensity values of MIP and NIP nanofilament dot arrays after synthesis, after template extraction, and after fluorescein adsorption (20 µM in DMSO). Measurements were done in triplicate, the error bars represent the standard error of the mean. The intensity values measured on porous microdots after fluorescein adsorption were added for comparison in E.

were purchased from Sigma-Aldrich. 4-VPy was vacuum-distilled before use. Fluorescein isothiocyanate Isomer I (FITC), and myoglobin from horse skeletal muscle were obtained from Sigma-Aldrich and fluorescein free acid from Fluka. For fluorescent microscopy measurements myoglobin was FITC-labeled following a standard protocol[20] optimized in our laboratory. Anhydrous dimethyl sulfoxyde (DMSO) was obtained from Sigma-Aldrich, the rest of the organic solvents used were of Chromasolv quality and used without further purification. Ultrapure water was produced with a RiOs Progard 2 Silver and a Milli-Q Q-Gard 1 systems from Millipore.

Silanization of Glass Substrates: Microscope glass slides (76 mm × 26 mm × 1 mm) were cut in half and placed into ceramic boxes for washing and activation steps. Cleaning of the slides was performed by successive washings at 90 °C for 10 min with an NH_3 aqueous solution (10% v/v), H_2O_2 in water (10% v/v) and finally with an aqueous solution of HCl (10% v/v) and H_2O_2 (10% v/v). The slides were afterwards washed twice with ultrapure water, acetone and finally toluene prior to the activation step. The slides were incubated overnight in a solution of MAPTMS in dry toluene (2% v/v), rinsed with toluene and acetone, and dried under a N_2 stream. The activated glass substrates were kept in a dry place, protected from light and used during one month following preparation.

Nanoporous Aluminium Oxides: The synthesis of the porous alumina surfaces was based on a previously published protocol[21] that has been modified for our needs.[18,19] In short, commercial aluminium substrates (80 mm × 30 mm × 0.3 mm) were annealed at 400 °C for 2 h in order to reorganize its crystalline structure and eliminate possible impurities. One aluminium plate was then connected to the anode of a power supply, the cathode being a stainless-steel plate of the same size, and submerged in an oxalic acid aqueous solution (0.5% w/v) at 5 °C. The substrate was subjected to anodization for 6 min at 110 V, resulting in the deposition of a thin Al_2O_3 layer. After rinsing the substrate with ultrapure water, this oxide layer was removed by immersing the plate for 45 min in a boiling 20% aqueous solution of acetic acid. The plate was then electro-oxidized again in the same oxalic acid bath at 110 V during 4 min. This treatment results in the deposition of a new Al_2O_3 layer with a better organization than the previous one. Finally, the substrate was immersed in a phosphoric acid aqueous solution (5% v/v) at 30 °C for 50 min. These conditions have been experimentally determined to yield an Al_2O_3 layer of approximately 5 µm thickness and a pore diameter of 150 nm.

Template Immobilization: Immobilization of fluorescein and myoglobin on the walls of the alumina pores was done as described in a previous paper.[18] For fluorescein, amino groups were generated at the inner surface of the porous Al_2O_3 layer by incubation of the substrates in a glass desiccator under a saturated atmosphere with APTES during 12 h, followed by rinsing with acetone and drying under a stream of nitrogen. The silanized alumina surface was then incubated in a solution of FITC in anhydrous DMSO (1 mg mL^{-1}) for 2 h, followed by washing with DMSO, acetone, and dried under a nitrogen stream. The success of the coupling was confirmed by fluorescence microscopy.

For myoglobin immobilization, the alumina substrates were silanized by immersion in a solution consisting of a mixture of of APTES (6.7 mL), ethanol (40.5 mL) and sodium acetate buffer (2.7 mL, 50 mM, pH 5.0) for 5 min. The substrates were briefly rinsed in pure ethanol and cured at 150 °C during 2 h. The silanization step was confirmed by FTIR measurements. The amino-modified alumina was reacted with glutaraldehyde, which acts as a linker molecule for the covalent immobilization of the protein. Thus, the modified nanoporous alumina substrates were incubated in a solution of glutaraldehyde (0.2 M) in phosphate buffer (50 mM, pH 7.0) at room temperature for 2 h, rinsed in ethanol, and dried under a stream of nitrogen. The substrates were then incubated overnight in a myoglobin solution (2 mg mL^{-1} in phosphate buffer 50 mM pH 7.0) at room temperature under gentle agitation. The

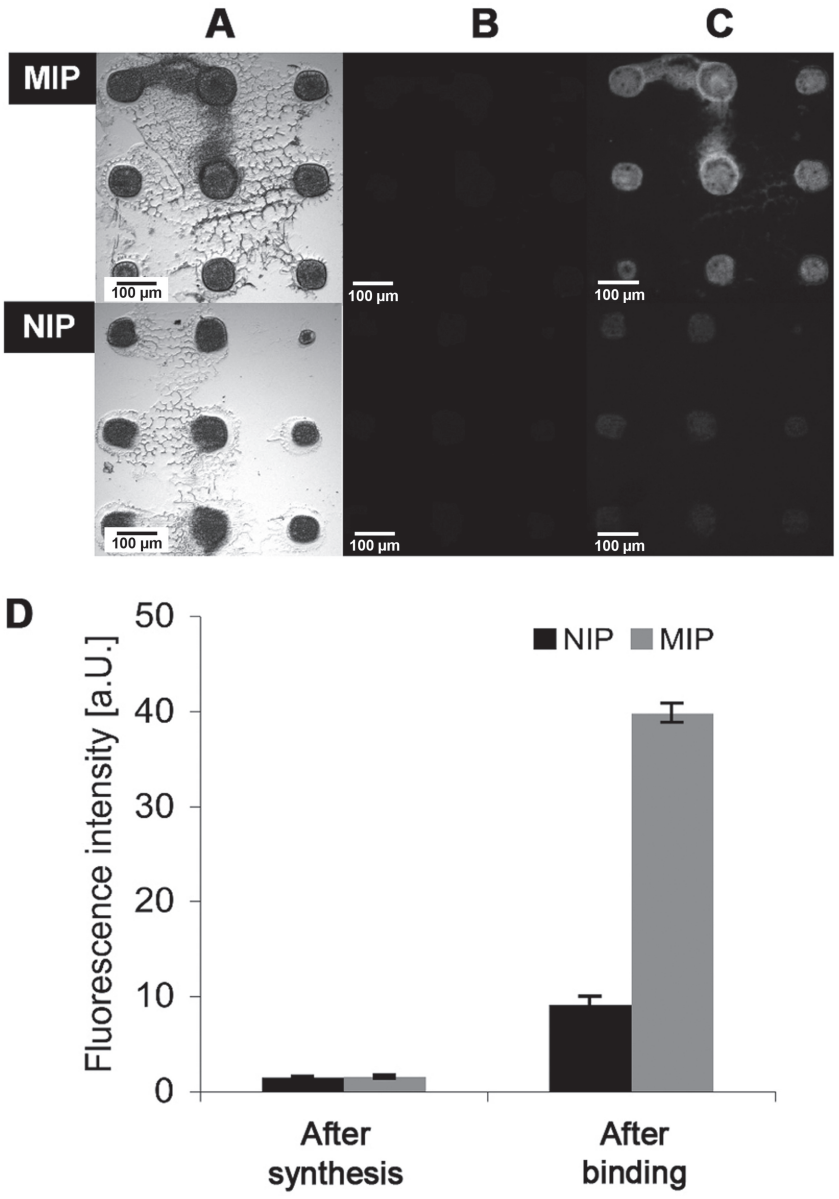

Figure 8. Optical microscope images of myoglobin imprinted and nonimprinted nanofilament dot arrays. Patterns were obtained using a mask with 0.5 mm × 0.5 mm features and a pitch of 2 mm. A) Bright-field images; B) fluorescence images after synthesis and template removal; C) fluorescence images after FITC–myoglobin adsorption (1 µM in phosphate buffer, 50 mM, pH 7.0). Exposure time 250 ms; D) Fluorescence intensity values of myoglobin imprinted and nonimprinted nanostructured dots after synthesis and after adsorption of FITC–myoglobin (1 µM in phosphate buffer, 50 mM, pH 7.0). Measurements were done in triplicate, the error bars represent the standard error of the mean.

substrates were then thoroughly rinsed with ultrapure water and used the same day. Myoglobin immobilization was confirmed by FTIR measurements.

Synthesis of MIP Arrays by Microscope Projection Photolithography: Photomasks (11 mm × 11 mm) were created using common graphic software, and printed on transparent acetate sheet (overhead transparency) with a thickness of 0.12 mm using a 1200 dots per inch ink-jet printer. The printed mask was afterwards inserted in the field diaphragm plane of the microscope, a Zeiss AxioTech Vario. Examples of the photomasks used are shown in the Supporting Information (Figure SI1). The light from a 100 W Hg lamp was filtered with an IR mirror to cut off wavelengths longer than 700 nm, thus avoiding undesired thermal polymerization. The exposure time was optimized for each photomask and MIP precursors mixture used. The objective used had a 10× magnification with NA = 0.2.

Fluorescein imprinted microdots were prepared from a mixture of fluorescein (0.25 mmol), 4-VPy (0.5 mmol), MMA (0.5 mmol), TRIM (2 mmol), DPAP (0.07 mmol), and 745 µL of a 0.1% PVAc solution in anhydrous DMSO. The nonimprinted dots were prepared from the same mixture in the absence of fluorescein. 5 µL of the abovementioned MIP precursors mixture were placed on a microscope glass slide and covered with a 5 mm × 26 mm slide of activated glass. The sandwich was placed on the sample stage of the microscope, which was focused on the space between the activated glass and the microscope slide. Polymerization was triggered by irradiation with the Hg lamp, projecting the pattern of the photomask through the 10× objective. Different polymerization times were tested from 10–180 s, the best patterns were obtained with 120 s. After polymerization, the glass slides were separated after rinsing with ethanol to remove the unreacted monomers. The activated glass slide was recovered bearing the pattern at its surface, rinsed again with ethanol and dried under a nitrogen stream.

Fluorescein and myoglobin imprinted nanostructured dots were obtained using nanoporous alumina substrates. The different imprinting templates were previously immobilized on these supports as described above. For fluorescein imprinting the MIP precursors mixture used was composed of 4-VPy (0.5 mmol), MMA (0.5 mmol), TRIM (2 mmol), DPAP (0.07 mmol). For imprinting of myoglobin, the composition was HEMA (0.5 mmol), MAA (0.5 mmol), TEGDMA (2 mmol), and DPAP (0.05 mmol). The porous alumina substrates were cut into 5 mm × 5 mm squares, one square was placed on a microscope glass slide, the alumina side facing up, and 1 µL of the MIP precursors solution was deposited and covered with a 5 mm × 26 mm activated glass slide. The system was placed on the stage of the microscope, which was focused on the interface between the alumina and the activated glass. Polymerization was initiated by irradiation with the Hg lamp through the photomask for a time between 180 and 300 s. After polymerization, the assembly was rinsed with ethanol and placed in an aqueous solution HCl (5 M) and $CuCl_2$ (0.2 M) to remove the aluminium layer. The alumina layer was subsequently dissolved by incubation in NaOH (0.2 M) at 40 °C for 2 h under agitation. The fluorescein template was removed by three incubations in a methanol/acetic acid (4:1) solution during

4 h, followed by three incubations in methanol. The effectiveness of the wash was confirmed by fluorescence microscopy. In the case of myoglobin MIPs, the nanostructured arrays were washed overnight in an SDS (10% w/v) and acetic acid (10% v/v) aqueous solution, and finally washed with ultrapure water for 30 min.

Binding Studies: In the case of fluorescein adsorption, the imprinted and nonimprinted polymer arrays were incubated in a fluorescein solution (5 mL) at appropriate concentration in DMSO for 2 h, in the dark under gentle agitation. The substrates were then briefly rinsed with acetone and dried under a nitrogen stream prior to analysis.

In the case of FITC–myoglobin adsorption, each substrate was incubated in a FITC–myoglobin solution (5 mL) at appropriate concentration in phosphate buffer (50 mM, pH 7.0), at room temperature for 12 h. The substrates were rinsed with phosphate buffer and allowed to dry at room temperature in the dark. The amount of target molecule adsorbed by the imprinted and nonimprinted arrays was evaluated by fluorescence intensity measurements using a Leica DMI6000 B fluorescence microscope with a 480 nm excitation filter and a 527 nm emission filter for both templates. The imaging parameters such as exposure time, gain, and intensity were kept constant during the same experiment for both imprinted and nonimprinted polymers. Fluorescence images of the samples were thus taken following extraction and re-adsorption of the template. The fluorescence intensity (FI) of the imprinted polymer was compared with that of the nonimprinted one, yielding the imprinting factor (IF) = FI_{MIP}/FI_{NIP}. The fluorescence intensity values were calculated with ImageJ software (public domain, http://rsb.info.nih.gov/ij/).

Characterization of the Arrays: The arrays were characterized by SEM using a Philips XL30 ESEM-FEG microscope. The deposition on the substrates of a 10 nm Au film was required prior to analysis.

Supporting Information

Supporting Information is available from the Wiley Online Library or from the author.

Acknowledgements

K.H., L.A.G., and A.V.L. gratefully acknowledge financial support from the European Union (Marie Curie Research Training Network NASCENT, Grant No. MRTN-CT-2006-33873). K.H. and A.L. thank the European Union for co-funding of equipment within the CPER 2007-2013. The authors thank Mr. Frédéric Nadaud from the Physico-chemical Analysis Unit at UTC.

[1] V. Espina, A. I. Mehta, M. E. Winters, V. Calvert, J. Wulfkuhle, E. Petricoin, L. A. Liotta, *Proteomics* **2003**, *3*, 2091.
[2] A. Lueking, D. J. Cahill, S. Mullner, *Drug Discov. Today* **2005**, *10*, 789.
[3] M. Lynch, C. Mosher, J. Huff, S. Nettikadan, J. Johnson, E. Henderson, *Proteomics* **2004**, *4*, 1695.
[4] K. Jain, *Curr. Opin. Drug Discov. Dev.* **2004**, *7*, 285.
[5] G. Vlatakis, L. I. Andersson, R. Muller, K. Mosbach, *Nature* **1993**, *361*, 645.
[6] K. Haupt, *Chem. Commun.* **2003**, 171.
[7] B. D. Gates, Q. Xu, J. C. Love, D. B. Wolfe, G. M. Whitesides, *Annu. Rev. Mater. Res.* **2004**, *34*, 339.
[8] D. W. Palmer, S. K. Decker, *Rev. Sci. Instrum.* **1973**, *44*, 1621.
[9] J. Behm, K. Lykke, M. Pellin, J. Hemmingers, *Langmuir* **1996**, *12*, 2121.
[10] L. A. Kung, J. T. Groves, N. Ulman, S. G. Boxer, *Adv. Mater.* **2000**, *12*, 731.
[11] J. Love, D. Wolfe, H. Jacobs, G. Whitesides, *Langmuir* **2001**, *17*, 6005.
[12] P. G. Conrad, P. T. Nishimura, D. Aherne, B. J. Schwartz, D. Wu, N. Fang, X. Zhang, M. J. Roberts, K. J. Shea, *Adv. Mater.* **2003**, *15*, 1541.
[13] H. Huang, C. Lin, A. Joseph, Y. Lee, *J. Chromatogr. A* **2004**, *1027*, 263.
[14] H. Huang, S. Huang, C. Lin, Y. Lee, *Anal. Chim. Acta* **2007**, *582*, 137.
[15] S. Guillon, R. Lemaire, A. V. Linares, K. Haupt, C. Ayela, *Lab Chip* **2009**, *9*, 2987.
[16] R. Schmidt, K. Haupt, *Chem. Mater.* **2005**, *17*, 1007.
[17] A. Belmont, S. Jaeger, D. Knopp, R. Niessner, G. Gauglitz, K. Haupt, *Biosens. Bioelectron.* **2007**, *22*, 3267.
[18] A. V. Linares, F. Vandevelde, J. Pantigny, A. Falcimaigne-Cordin, K. Haupt, *Adv. Funct. Mater.* **2009**, *19*, 1.
[19] F. Vandevelde, A. S. Belmont, J. Pantigny, K. Haupt, *Adv. Mater.* **2007**, *19*, 3717.
[20] S. Papadopoulos, V. Endeward, B. Revesz-Walker, K. D. Jürgens, G. Gros, *Proc. Nat. Acad. Sci. USA* **2001**, *98*, 5904.
[21] H. Masuda, K. Fukuda, *Science* **1995**, *268*, 1466.

Received: February 3, 2011
Revised: March 9, 2011
Published online: June 21, 2011